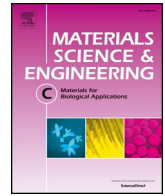




Since January 2020 Elsevier has created a COVID-19 resource centre with free information in English and Mandarin on the novel coronavirus COVID-19. The COVID-19 resource centre is hosted on Elsevier Connect, the company's public news and information website.

Elsevier hereby grants permission to make all its COVID-19-related research that is available on the COVID-19 resource centre - including this research content - immediately available in PubMed Central and other publicly funded repositories, such as the WHO COVID database with rights for unrestricted research re-use and analyses in any form or by any means with acknowledgement of the original source. These permissions are granted for free by Elsevier for as long as the COVID-19 resource centre remains active.



Interleukin-4 assisted calcium-strontium-zinc-phosphate coating induces controllable macrophage polarization and promotes osseointegration on titanium implant

Da-Wang Zhao^{a,b,c,1}, Kang-Qing Zuo^{d,1}, Kai Wang^d, Zhao-Yang Sun^{c,e,f}, Yu-Peng Lu^d, Lei Cheng^{a,*}, Gui-Yong Xiao^{d,*}, Chao Liu^{c,e,**}

^a Department of Orthopedics, Qilu Hospital of Shandong University, Jinan 250012, PR China

^b Cheeloo College of Medicine, Shandong University, Jinan 250012, PR China

^c Institute of Stomatology, Shandong University, Jinan, Shandong 250012, PR China

^d School of Materials Science and Engineering, Shandong University, Jinan 250061, PR China

^e Department of Oral and Maxillofacial Surgery, Qilu Hospital of Shandong University, Jinan 250012, PR China

^f School of Stomatology, Shandong University, Jinan 250012, PR China

ARTICLE INFO

Keywords:

Interleukin-4
Calcium-strontium-zinc-phosphate coating
Titanium
Osteoimmunomodulation
Orthopedic implants

ABSTRACT

Titanium (Ti) and its alloys are believed to be promising scaffold materials for dental and orthopedic implantation due to their ideal mechanical properties and biocompatibility. However, the host immune response always causes implant failures in the clinic. Surface modification of the Ti scaffold is an important factor in this process and has been widely studied to regulate the host immune response and to further promote bone regeneration. In this study, a calcium-strontium-zinc-phosphate (CSZP) coating was fabricated on a Ti implant surface by phosphate chemical conversion (PCC) technique, which modified the surface topography and element constituents. Here, we envisioned an accurate immunomodulation strategy via delivery of interleukin (IL)-4 to promote CSZP-mediated bone regeneration. IL-4 (0 and 40 ng/mL) was used to regulate immune response of macrophages. The mechanical properties, biocompatibility, osteogenesis, and anti-inflammatory properties were evaluated. The results showed that the CSZP coating exhibited a significant enhancement in surface roughness and hydrophilicity, but no obvious changes in proliferation or apoptosis of bone marrow mesenchymal stem cells (BMMSCs) and macrophages. In vitro, the mRNA and protein expression of osteogenic related factors in BMMSCs cultured on a CSZP coating, such as ALP and OCN, were significantly higher than those on bare Ti. In vivo, there was no enhanced bone formation but increased macrophage type 1 (M1) polarization on the CSZP coating. IL-4 could induce M2 polarization and promote osteogenesis of BMMSCs on CSZP in vivo and in vitro. In conclusion, the CSZP coating is an effective scaffold for BMMSCs osteogenesis, and IL-4 presents the additional advantage of modulating the immune response for bone regeneration on the CSZP coating in vivo.

1. Introduction

Titanium (Ti) and its alloy-based implants have dominated the medical market of orthopedic and dental implantation in the world given their good biocompatibility and mechanical properties [1,2]. However, the mechanical and biological properties of Ti implants can affect osseointegration in response to the host immune response. To obtain better osseointegration of Ti implants, several surface modification techniques have been studied systematically to improve

surface morphology and element constituents to obtain better osteoimmunomodulation properties, and these include plasma spraying, sol-gel, magnetron sputtering, biomimetic precipitation, and chemical conversion. [3–6].

However, the host's body is a complex environment, and the implantation will inevitably lead to a series of biological responses. Depending on context dependent polarization profiles, macrophages may be responsible for these responses [7,8]. Signals from various surfaces of Ti implant may trigger the switching or polarization of

* Corresponding authors.

** Correspondence to: C. Liu, Institute of Stomatology, Shandong University, Jinan, Shandong 250012, PR China.

E-mail addresses: chenglei@email.sdu.edu.cn (L. Cheng), xiaoguiyong@sdu.edu.cn (G.-Y. Xiao), qiluliuchao@sdu.edu.cn (C. Liu).

¹ These authors contributed equally to this work.

macrophage phenotypes associated with the immune response, followed by pro-osteogenic signaling. These findings demonstrated that surface modification methods for osseointegration should concentrate not only on osteogenesis but also on immunomodulation to build an optimal environment. Therefore, the osteoimmunomodulation capacity becomes a principal factor for the evaluation of surface modification of Ti implants.

The phosphate chemical conversion (PCC) technique is a chemical and electrochemical process of forming PCC coatings and firmly binds to the substrate. The PCC coating synthesized directly on the Ti implant surface can not only regulate wear- and corrosion-resistance, adhesion, roughness, and hydrophilicity, but also couples elements such as calcium (Ca), zinc (Zn), strontium (Sr) into the coating [9–12]. As the main component of human bone, Ca is used in synthesis and application of various biomaterials [8,13]. Sr is a stimulus to bone formation and the main component of drugs for the treatment of osteoporosis [14]. Zn is essential for the immune response, and an optimal dose of Zn creates an anti-inflammatory environment by promoting the expression of anti-inflammatory factors [15]. In theory, a Ca-Sr-Zn-P (CSZP) coating synthesized by PCC method should act as a promising surface for osseointegration of Ti implants by regulating the immune response.

Macrophage polarization plays an important role in scaffold-induced osteoimmunomodulation. Acute inflammation is the first stage of tissue healing [16], type 1 macrophages (M1) have traditionally been regarded as inflammatory cells at this stage and produce a fibrous encapsulation to protect the host [17]. Instead, type 2 macrophages (M2) generally act to inhibit the development of inflammation and promote osteogenic growth factors from the third day post-implantation. It has been reported that an accurate coordination of M1 and M2 surrounding the scaffold will further optimize the osteoimmunomodulatory effect, and thus enhance the osteogenesis and related angiogenesis [18]. Therefore, supplementing external factors at an appropriate timepoint to drive macrophage polarization is a good approach to improve osteoimmunomodulation. As a regulator of M2 polarization, interleukin (IL)-4 has been shown to have a good regulatory effect on the M1/M2 ratio at appropriate doses and time points without any interference on osteogenic differentiation of stem cells. IL-4 may be a suitable auxiliary reagent to be applied for CSZP immune regulation.

In this study, the PCC technique was used to synthesize a CSZP coating on the surface of Ti implants. The mechanical properties and osteoimmunomodulation capacity of CSZP were investigated. Meanwhile, the diverse roles of BMMSCs and macrophages in this phenomenon were evaluated to identify any potential mechanisms. The aim of our study was to elucidate the application of PCC coating on Ti implants for osteoimmunomodulation.

2. Materials and methods

2.1. Specimen preparation

Commercial grade pure Grade II titanium (CP Ti, TA2) was used in this study as substrates for characterization. The pure Ti rods were wire-cut into specimens with the dimensions of $\Phi 10 \times 3$ mm and followed by grinding with a series of silicon carbide (SiC) papers up to 2000 grit, and subsequently rinsed with gasoline, acetone, alcohol, and deionized water in an ultrasonic bath, respectively. Prior to PCC treatment, the above Ti specimens were first connected with pure Fe clips to form a sort of galvanic coupling system as described in our previous study [19], and then were pickled with 2 wt% hydrofluoric acid (HF) and 3 g/L colloidal titanium phosphate at 25 °C for 30 s for surface activation, respectively. Immediately, the as-pretreated coupled samples were immersed in PCC solution with compositions of $\text{SrCl}_2 \cdot 6\text{H}_2\text{O}$: 32 g/L, $\text{Ca}(\text{NO}_3)_2 \cdot 4\text{H}_2\text{O}$: 12 g/L, $\text{NaH}_2\text{PO}_4 \cdot 2\text{H}_2\text{O}$: 24 g/L, $\text{Zn}(\text{H}_2\text{PO}_4)_2 \cdot 2\text{H}_2\text{O}$: 0.7 g/L, NaNO_3 : 2 g/L, and the pH of the solution was adjusted to 3.25 using H_3PO_4 or NaOH. Meanwhile, ultrasonic irradiation (UI) was performed by placing the reaction beakers into

ultrasonic cleaners with an output power of 240 W to promote coating formation. Following PCC, the coated Ti specimens were washed with deionized water and dried at 40 °C for further characterization.

2.2. Coating characterization

A field emission scanning electron microscopy (FE-SEM, JSM-7800F, JEOL, Japan) equipped with an energy dispersive X-spectroscopy (EDS, Oxford XMax-80) was used to observe the surface morphology and to detect elemental composition of the coating. The cross-section of the coating was prepared in an ion milling system (IB-19510CP, JEOL, Japan) with ion beam energy of 6 keV. The phase composition analysis of the coating was carried out using a D/max- γ B X-ray diffractometer (XRD, Rigaku, Japan) operated at 40 kV and 100 mA, which used Cu-K α radiation at a scan speed of 4° min⁻¹ from 10° to 90° at a 2 θ angle. The surface topography and roughness of the bare and coated Ti were evaluated by an atomic force microscopy (AFM, Dimension Icon, Veeco Instruments Inc., USA) operating in the tapping mode in air, while three-dimensional (3D) images were recorded using a SiNi tip with a nominal spring constant of 42 Nm⁻¹ within a scan area of 10 × 10 μm . Roughness values (Ra) were calculated using NanoScope Analysis software (version 1.5). The wettability of the bare and coated Ti specimens was tested using an overall rotation contact angle instrument (DSA100S, KRÜSS, Germany) according to the sessile drop method at room temperature and 36%–40% humidity. The release profiles of Ca^{2+} , Sr^{2+} and Zn^{2+} from the CSZP coating were studied in phosphate buffered saline (PBS). The samples were placed in 10 mL of new PBS medium, and incubated at 37 °C under continuous shaking at 100 rpm for 1, 4, 7, 10, and 14 days. At the end of each preset time point, all the leachates were removed and replaced with fresh medium aliquots. The amounts of Ca^{2+} , Sr^{2+} and Zn^{2+} were analyzed with an ICP-OES (ICP-OES730, Agilent, Japan). All roughness, wettability, and ion release evaluation were performed in triplicate to ensure the reliability of the results.

2.3. Reagents

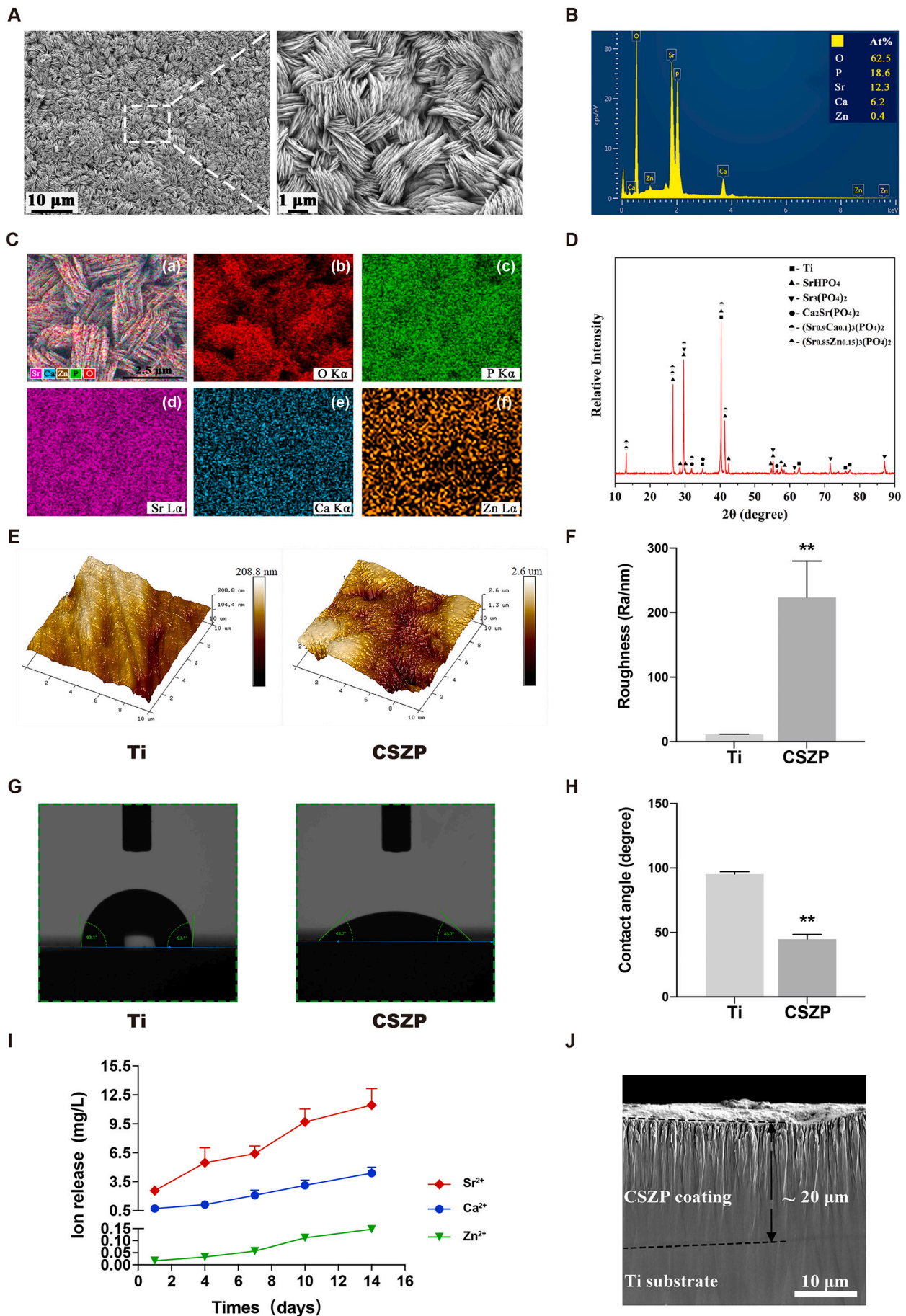
Mouse anti-iNOS (ab49999), Rabbit anti-Mannose Receptor (ab64693), Mouse anti-Osteocalcin (ab13420), Rabbit anti-Alkaline Phosphatase (ab218574) were obtained from abcam, USA; DyLight 488, Goat Anti-Mouse IgG (A23210, Abbkine, USA); DyLight 594, Goat Anti-Rabbit IgG (A23420, Abbkine, USA); Phalloidine (40735ES75, YEASEN, China); DAPI (C1005, Beyotime, China); M-CSF (400-28, Peprotech, USA); IL-4 (400-04, Peprotech, USA).

2.4. Rat bone marrow mesenchymal stem cells isolation and culture

All animal experiments complied with the ARRIVE guidelines and were carried out in accordance with the National Institutes of Health guide for the care and use of Laboratory animals (NIH Publications No. 8023, revised 1978). As previously described [20], bone marrow mesenchymal stem cells (BMMSCs) were obtained from 4-week-old male Sprague-Dawley rats. BMMSCs were cultured in DMEM (Gibco, USA) supplemented with 10% fetal bovine serum (FBS, Gibco, USA), 100 U/mL penicillin and 100 $\mu\text{g}/\text{mL}$ streptomycin (Gibco, USA) and incubated in 5% CO₂ atmosphere at 37 °C. A volume of 1 mL BMMSCs suspension was added gently on scaffolds positioned in 24-well plates. BMMSCs on the scaffolds were cultured in medium for the desired time points for all of the following experiments.

2.5. Rat bone marrow cells-derived macrophage isolation and culture

The method of obtaining macrophages is the same with that of BMMSCs, with the difference that the medium required supplementation with 30 ng/mL of M-CSF (400-28, Peprotech, USA). A 1 mL rat macrophage suspension was added gently onto scaffolds in the 24-well



(caption on next page)

Fig. 1. Characterization of the CSZP coating on Ti implants.

- A. Surface morphologies revealed by SEM.
- B. The EDS spectra and relative contents of each element.
- C. Surface distribution of each element.
- D. Phase compositions by XRD spectrum.
- E. Surface 3D topographies by AFM.
- F. Surface roughness (Ra).
- G. Water droplet shapes.
- H. Water contact angles.
- I. Release profiles of Ca^{2+} , Sr^{2+} , and Zn^{2+} .
- J. SEM image of the coating cross-section.

plate. Rat macrophages growing on the scaffolds were cultured in medium for the desired timepoints for all of the following experiments.

2.6. Co-culture system

BMMSCs ($3 \times 10^4/\text{mL}$) and macrophages ($3 \times 10^4/\text{mL}$) were mixed together and seeded onto the scaffolds in the 24-well plate. The medium in the CSZP + IL-4 group was supplemented with 40 ng/mL IL-4 (Peprotech, USA) to mimic the biological transition from M1 to M2 polarization. Culture medium was changed every two days.

2.7. Immunofluorescence staining

After BMMSCs ($3 \times 10^4/\text{mL}$) or macrophages ($3 \times 10^4/\text{mL}$) were cultured on the surface of the scaffold for 2 days, the nuclei were stained with DAPI and the actin filaments were stained with phalloidine and assessed by Immunofluorescence (IF).

In order to judge the effect of scaffolds on the osteogenesis of BMMSCs at the protein level, we selected two osteogenic indicators, ALP and OCN, and performed IF staining to determine the osteogenic ability of different scaffolds. After BMMSCs ($3 \times 10^4/\text{mL}$) were cultured on the surface of the scaffold for a certain period of time, they were fixed, incubated with primary and secondary antibodies, and stained the nucleus and actin filaments in sequence.

To determine the polarization of macrophages on the scaffolds, iNOS and CD206 were used as the M1 and M2 polarization surface markers, respectively. IF staining was performed as described above. Finally, cell adhesion morphology and protein expression were observed under a confocal microscope (Opera Phenix, PerkinElmer, USA).

2.8. Cell proliferation and apoptosis

After the cells ($3 \times 10^4/\text{mL}$) were cultured on the surface of the scaffold for 2, 4, 6, and 8 days, the cell number was counted by cytometry.

In order to assess apoptosis, the BMMSCs (2×10^6) were harvested after one day of incubation, and were then stained with Annexin V and Propidium Iodide. A Gallios flow cytometer (Beckman, USA) was used to determine the percentage of dead and apoptotic cells of each group.

2.9. Reverse transcription-polymerase chain reaction

After the cells ($3 \times 10^4/\text{mL}$) were cultured for 48 h, mRNA was extracted and reverse transcribed into complementary DNA. In accordance with the manufacturer's instructions, of SYBR Green Realtime PCR Master Mix (QPK-201, Toyobo, Japan), Reverse transcription-polymerase chain reaction (RT-PCR) was performed to reveal any fold changes in the expression of selected genes on samples exposed to Ti compared to control cells.

2.10. RT-PCR primers

ALP F: ATGCTCAGGACAGGATCAAA; R: CGGGACATAAGCGAGTT TCT.

COL1 F: AGCTCGATACACAATGGCT; R: AGCTCGATACACAATGG CCT.

OCN F: CAGACAAGTCCCACACAGCA; R: CCAGCAGAGTGAGCAGA GAG.

RUNX2 F: ATCATTCAGTGACACCACCA; R: GTAGGGGCTAAAGGC AAAAG.

β actin F: CCTCTATGACAACACAGT; R: AGCCACCAATCCACACAG.

CCR7 F: CATTTTCCAGGTGTGCTTCTGC; R: CACCGACTCATACAG GGTGT.

CD206 F: GAGGACTGCGTGGTGATGAA; R: CATGCCGTTTCCAGCC TTTC.

BMP2 F: GCATGTTTGGCCTGAAGCAG; R: CGATGGCTTCTTCGTG ATGG.

IL-1 β F: GCACCTTCTTTTCCTTCATCTTTG; R: TTTGTCGTTGCTTG TCTCTCCTT.

β actin F: CTCTGTGTGGATTGGTGGCT; R: CGCAGCTCAGTAACAG TCCG.

2.11. Rat subcutaneous implant model

Four-week-old rats were anesthetized by subcutaneous injection of 10% chloral hydrate. After skin preparation and draping, samples containing BMMSCs (2×10^4), which had been co-cultured for two days, was introduced onto the subcutaneous layer on the back incision, and the incisions were sutured layer by layer. All surgical operations were performed in an operating room under strong aseptic conditions.

At day 3 post-surgery, the rats of the Ti + IL-4 and CSZP + IL-4 groups were anesthetized, and 10 ng IL-4 (resuspended in 20 μL 0.9% NaCl) was injected through the skin directly over the scaffolds. Daily injection of IL-4 was performed from day 3 to day 7 as described previously [18].

After 2 weeks, the subcutaneous tissue surrounding the scaffold was removed and was used for subsequent experiments. Half of the subcutaneous tissue was used to extract mRNA and to carry out RT-PCR, as for the in vitro experiments. After fixation and embedding, tissue sections ($\approx 8 \mu\text{m}$) were prepared to quantify the portion of different phenotypes of macrophages in the fibrous layer by IF staining. In addition, paraffin sections were stained with hematoxylin and eosin (HE) to evaluate the inflammatory reaction of the materials.

2.12. Rat femoral defect repair model

A rat femoral defect repair model was used to investigate the capacity of bone repair in vivo ($n = 5$ per group). Cylindrical implants ($\Phi 2 \times 5 \text{ mm}$) were implanted into the rat femur. IL-4 was injected through the skin over the implant on day 3 post-surgery in the experimental group, daily injection was performed from day 3 to 7. To mark new bone formation, two fluorescent labels (Calcein green and Alizarin red) were injected into the tissue surrounding the implantation fields at weeks 2 and 4, respectively. After 6 weeks, the rats were euthanized and the femur was removed for micro-computed tomography (CT) and hard tissue slicing.

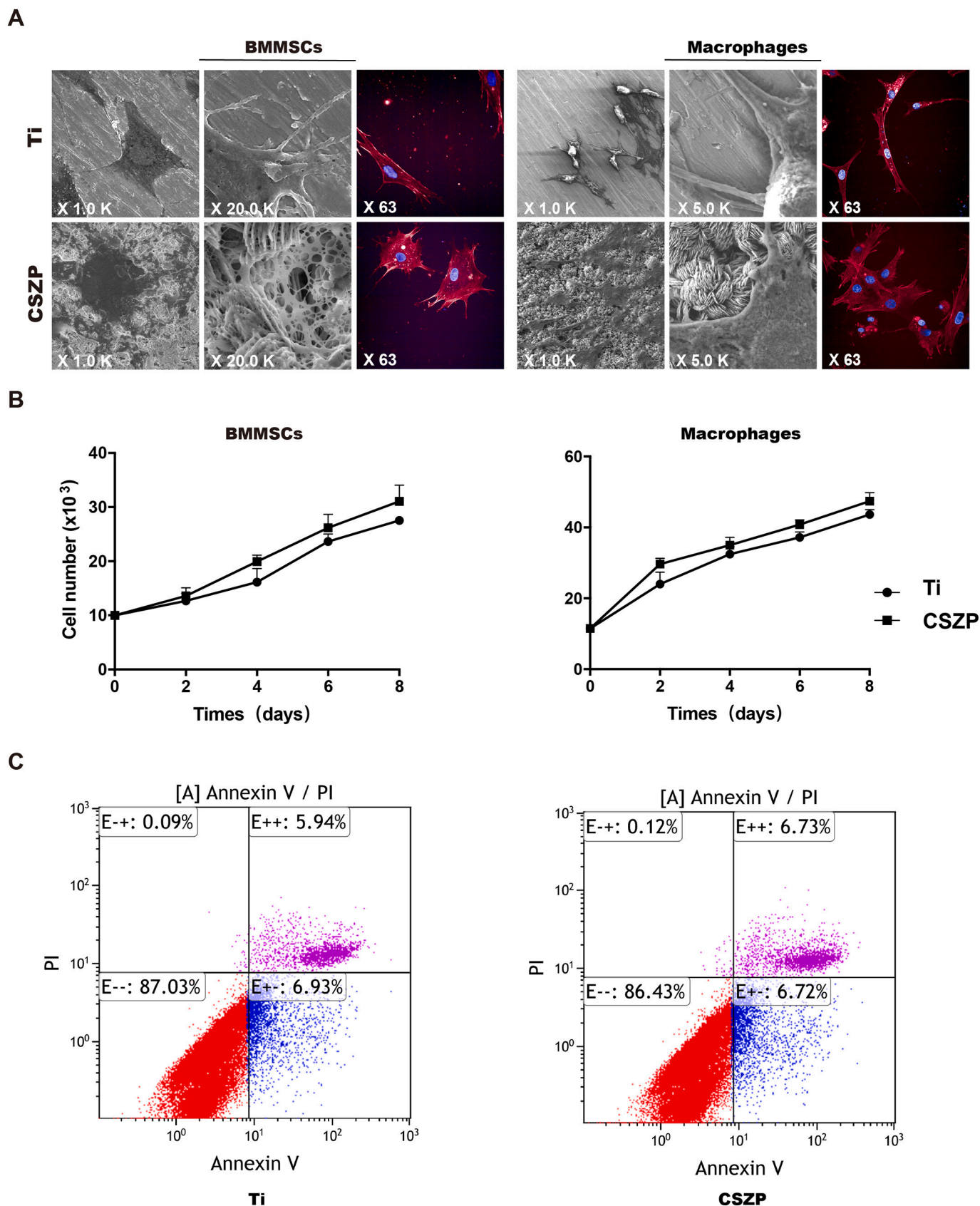
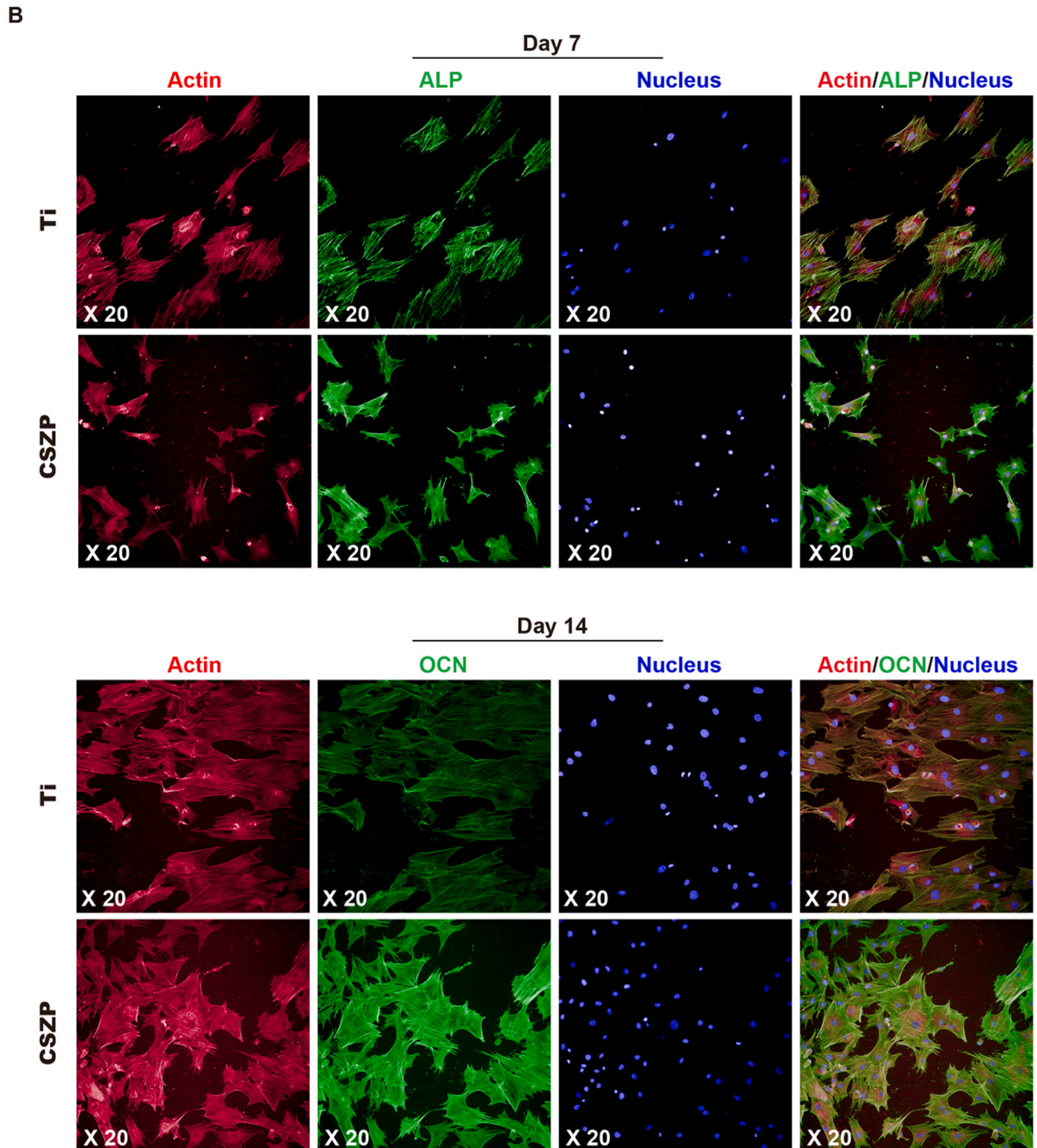
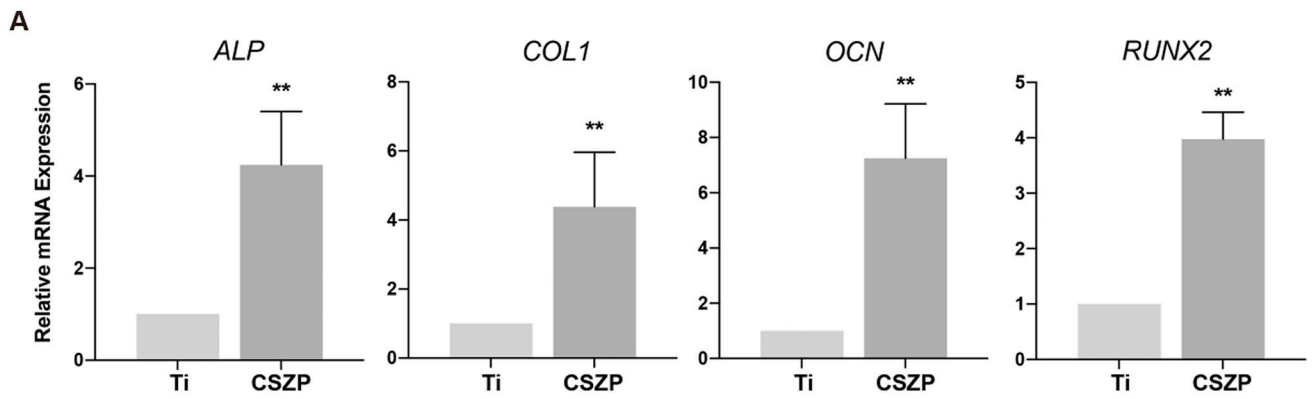


Fig. 2. CSZP coating on Ti implants exhibit good biocompatibility on BMMSCs and macrophages.
 A. Adhesion and morphology of BMMSCs and macrophages on samples by SEM and immunofluorescence staining.
 B. Proliferation of BMMSCs and macrophages cultured on samples.
 C. Percentages of apoptotic BMMSCs cultured on samples evaluated by flow cytometry.



(caption on next page)

Fig. 3. CSZP coating on Ti implants influences expression of osteogenesis genes and protein in BMMSCs.

A. Expression of *ALP*, *COL1*, *OCN* and *RUNX2* mRNA of BMMSC samples.
B. Expression of *ALP* and *OCN* immunofluorescent staining of BMMSC samples.

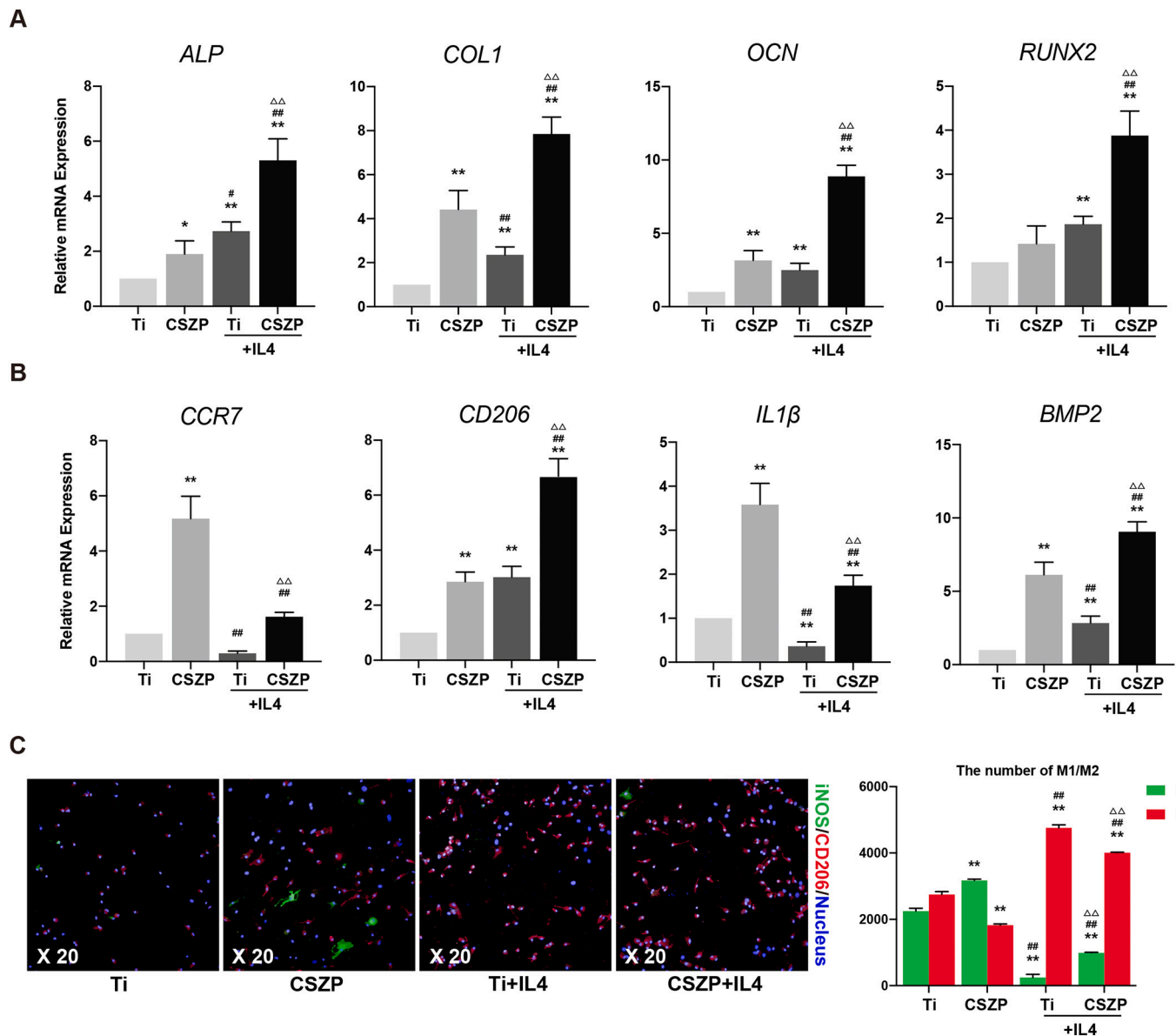


Fig. 4. CSZP coating on Ti implants exposed to IL-4 regulates osteogenesis of BMMSCs and macrophages polarization under co-culture system.

A. *ALP*, *COL1*, *OCN* and *RUNX2* mRNA expression determined by RT-PCR under co-culture system.
B. *CCR7*, *CD206*, *IL-1β* and *BMP2* mRNA expression determined by RT-PCR under co-culture system.
C. Immunofluorescent staining of cells under co-culture system.

2.13. Micro CT

The femurs were collected, and the attached soft tissue was removed thoroughly and fixed in 4% paraformaldehyde. The fixed femur with implants were analyzed using micro CT system (NMC-100, PINGSENG Healthcare Inc., China) at a resolution of 15 μm, a voltage of 90 kV, and a current of 80 μA. Threshold-based segmentation and 3D measurement analyses (BV/TV, TB/Th, TB/N) were performed using Avatar software 1.3.0 (PINGSENG Healthcare Inc., China).

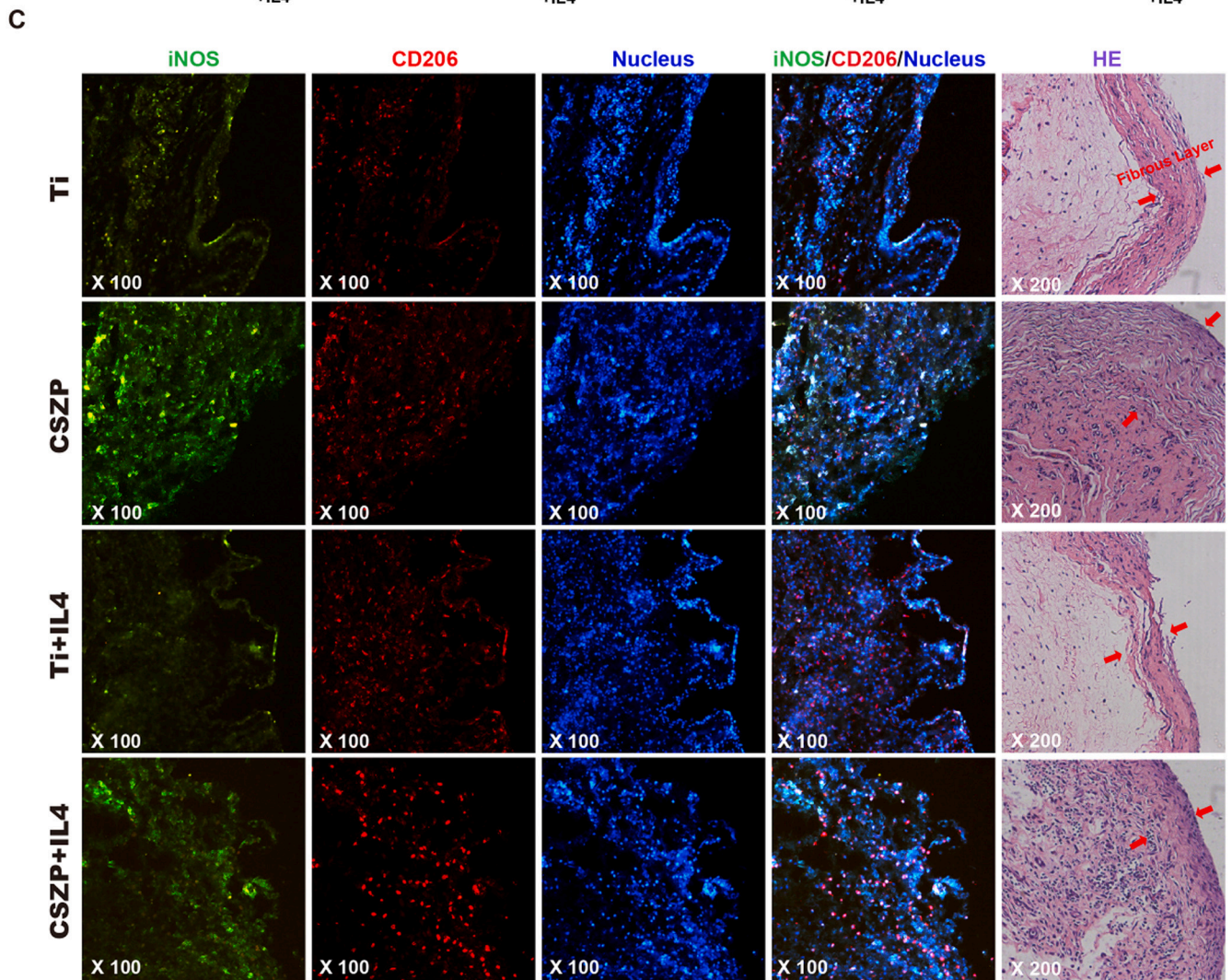
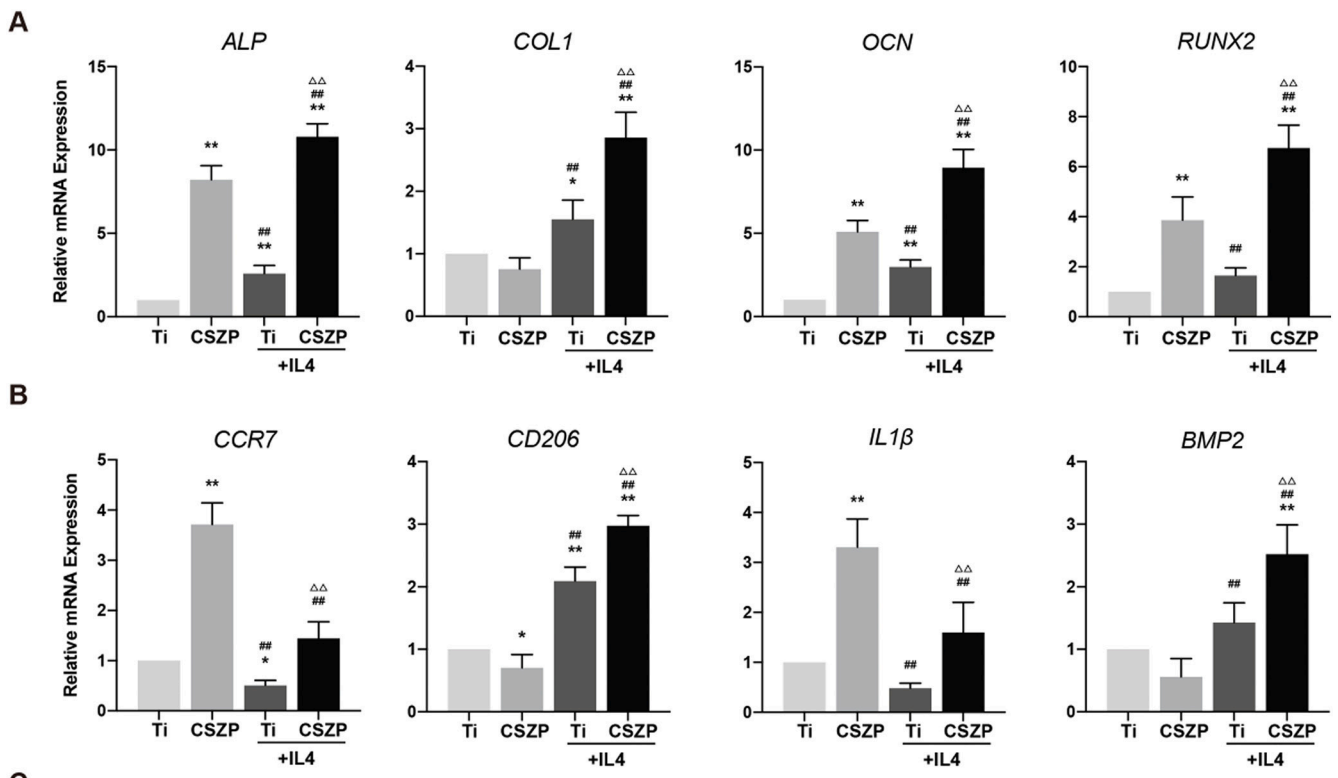
2.14. Hard-tissue slicing staining

The femurs with the samples were fixed and embedded, and cut into

30 μm thick sections across a transverse section of the implant. Then, the slide was stained with HE and toluidine blue (TB) to evaluate bone tissue surrounding the implant. Finally, the slide was rinsed under running water, covered and observed under a microscope.

Red field or blue field (indicating new bone formation) was considered positive area of HE or TB staining. The curve length of the contact surface between the new bone and the implant was considered the contact length. We used the result of a positive area/contact length as a quantitative indicator of new bone formation.

In order to quantify Calcein green and Alizarin red-marked osteogenesis, we calculated the area of the green field or red field by ImageJ 1.52 k software as the positive area of Calcein or Alizarin red respectively. We also calculated the area of the total field as the total area. We



(caption on next page)

Fig. 5. CSZP coating on Ti implants exposed to IL-4 in the subcutaneous implant model regulates macrophage polarization and osteogenesis associated genes.

A. Gene expression of *ALP*, *COL1*, *OCN* and *RUNX2* determined by RT-PCR.

B. Gene expression of *CCR7*, *CD206*, *IL-1 β* and *BMP2* determined by RT-PCR.

C. Immunofluorescent staining result of macrophages in subcutaneous tissue: red (CD206), green (iNOS), and blue (DAPI). HE staining of subcutaneous tissue. (For interpretation of the references to colour in this figure legend, the reader is referred to the web version of this article.)

used result of the calculated positive area/total area as a quantitative indicator of new bone formation at different stages (week 2 and week 4).

All digital images obtained from the stained sections were randomly chosen and analyzed using ImageJ 1.52 k software.

2.15. Microarray RNA-sequence

A microarray was used to detect changes in gene expression of macrophages on scaffolds. Macrophages were seeded on scaffolds (6×10^5 per well) and cultured for 4 days. Then, cell mRNA was harvested by TRIzol reagent, and overall gene expression was examined by the Lian Chuan Biotechnology Institute (LC, China). The Kyoto Encyclopedia of Genes and Genomes (KEGG) pathways or GO terms were used to provide detailed information on the genes associated with different biological functions in known signal or metabolism pathways. We identified the relationships between macrophage polarization and GO terms or KEGG pathways based on the constructed dataset.

2.16. Statistical analysis

Data are reported as mean \pm standard deviation. Differences among groups were analyzed by one-way ANOVA using SPSS Statistical software version 23. * $P < 0.05$ compared to Ti. ** $P < 0.01$ compared to Ti. # $P < 0.05$ compared to CSZP. ## $P < 0.01$ compared to CSZP. $\Delta P < 0.05$ compared to Ti + IL-4. $\Delta\Delta P < 0.01$ compared to Ti + IL-4.

3. Results

3.1. Fabrication and characteristics of CSZP-coated Ti implant

Fig. 1A displayed the surface micromorphology of this CSZP coating on pure Ti substrates obtained by PCC treatment. As shown in Fig. 1A, the entire surface of the Ti substrate was covered by a relatively loose coating composed of micellar lamellar crystals with no substrate exposed. The crystals of the CSZP coating were arranged regularly and orderly. Different micellar clusters were intersected and embedded with each other horizontally and stacked vertically with multiple layers. As can be seen from the high-magnification image in Fig. 1A, CSZP coating exhibited novel and unique crystal structure characteristics. Micellar clusters were composed of micro-nano lamellar crystals of regular shape and uniform size arranged in parallel, with the length of individual lamellar crystals being about 1–2 μm and the thickness about 100 nm. The FE-SEM images of the cross-section of the coating are presented in Fig. 1J. The thickness of the CSZP coating is around 20 μm , indicating that the coating is formed by a multilayer stack of micellar lamellar crystals perpendicular to the substrate. The element composition detection results of the CSZP coating are shown in Fig. 1B and C. Fig. 1B illustrates the EDS spectrum and relative content (atomic ratio), while Fig. 1C illustrates the distribution maps of each element. The CSZP coating mainly contained elemental O, P, Sr, Ca and trace Zn, while all elements were evenly distributed on the surface of the coating. The EDS results could prove that Sr, Ca, and Zn elements were successfully introduced into CSZP coating. In addition, higher contents of O and P elements also indicated that the coating was mainly composed of phosphate. The XRD pattern (Fig. 1D) revealed that the main phase compositions of the CSZP coating comprised strontium hydrogen phosphate (SrHPO_4) and strontium phosphate ($\text{Sr}_3(\text{PO}_4)_2$). Meanwhile,

due to the introduction of Ca and a small amount of Zn in the PCC solution, Ca and Zn ions could be doped into strontium phosphate crystals during the nucleation-growth process of phosphate crystals, forming Sr–Ca phosphate compounds including $(\text{Sr}_{0.9}\text{Ca}_{0.1})_3(\text{PO}_4)_2$ and $\text{SrCa}_2(\text{PO}_4)_2$, and trace amounts of strontium-zinc phosphate $(\text{Sr}_{0.85}\text{Zn}_{0.15})_3(\text{PO}_4)_2$, with different chemical ratios. Fig. 1E and F show the 3D topography and corresponding roughness value (Ra) calculation results of Ti and CSZP coating surfaces obtained by AFM. Obviously, the Ti surface displayed a typical parallel abrasive scratched morphology after sanding, with relatively smooth surface structure and small roughness value (11.1 ± 0.4 nm). By contrast, the CSZP coating displayed a rough surface with high and low undulations, and the visualized micellar layer lamellar crystal cluster structure was consistent with SEM results (Fig. 1A), and its surface roughness value was significantly larger than Ti, reaching a size of 223.3 ± 46.3 nm. Fig. 1G and H illustrate the shape of the water droplets on the Ti and CSZP coating surfaces and the corresponding contact angle calculation results. The water contact angle value of the Ti surface was $95.3 \pm 1.5^\circ$, showing hydrophobic properties, while the CSZP coating could dramatically improve wettability, and the water contact angle value was reduced to $44.9 \pm 3.0^\circ$, indicating that the CSZP coating had good hydrophilicity (Fig. 1H). Fig. 1I shows the amount of ion release results that were achieved by measuring the concentration of released Ca^{2+} , Sr^{2+} and Zn^{2+} at 1, 4, 7, 10, and 14 days from the CSZP coating after immersion in PBS. The results demonstrated that Ca^{2+} , Sr^{2+} , and Zn^{2+} exhibited slow and a continuous release over 14 days. Compared to the ion release results, the release amounts of Sr^{2+} and Ca^{2+} are notably higher than that of Zn^{2+} , which is consistent with the EDS element content results.

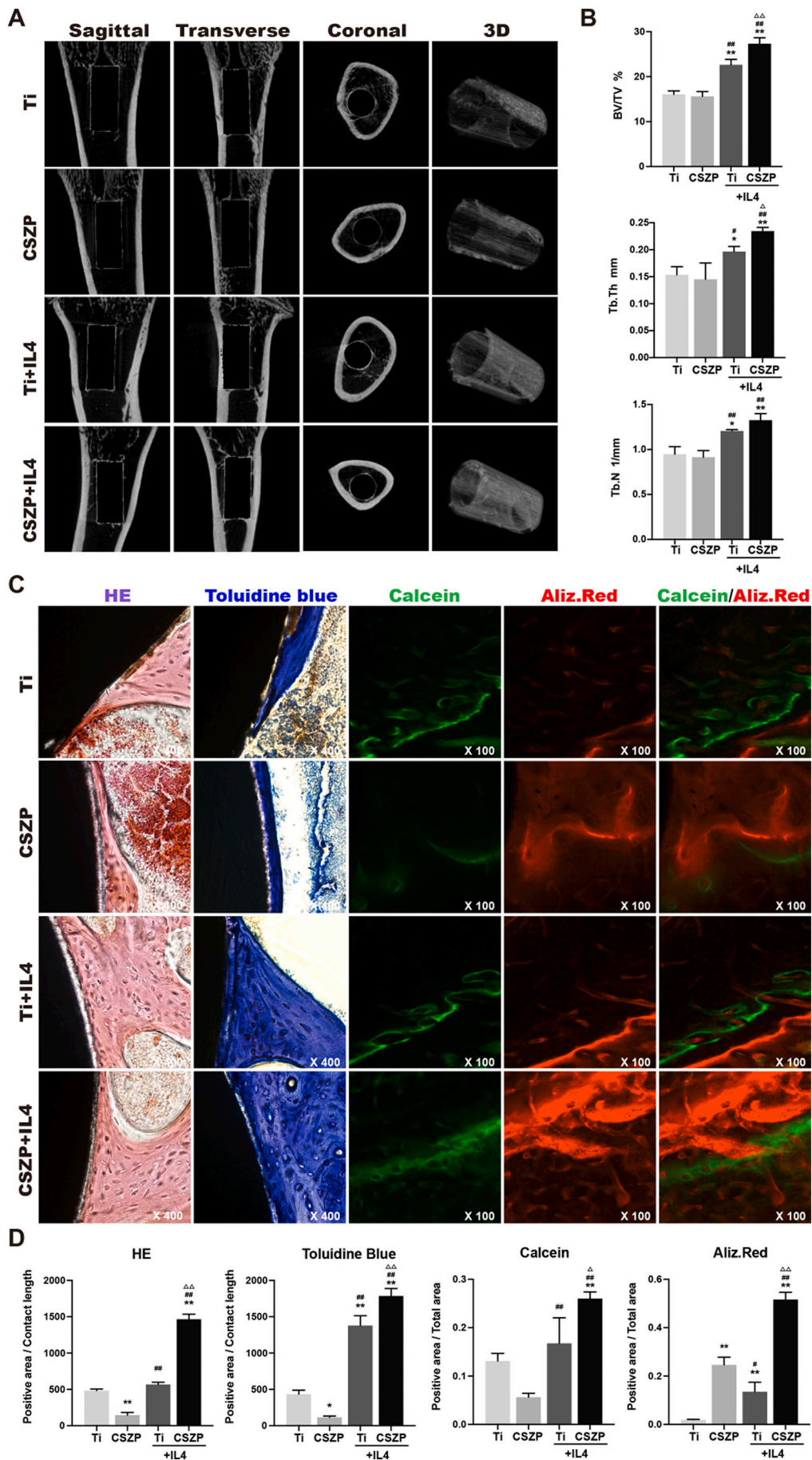
3.2. Evaluation of in vitro biocompatibility of the CSZP-coated Ti implant

The morphology of BMMSCs revealed polygon-like shapes obtained from the CSZP coating and spindle-like shapes on the bare Ti, while macrophages were spindle-like on both Ti and CSZP coating (Fig. 2A). There were more extended pseudopodia of BMMSCs on the CSZP coating than that on the Ti scaffolds. Compared with macrophages on the Ti scaffolds, the sizes of the macrophages were wider on the CSZP-coated implants. However, we could not find any significant differences on cell proliferation or apoptosis between these two samples (Fig. 2B and C). Although the morphologies of BMMSCs and macrophages on Ti and CSZP were variable, the biocompatibility of CSZP coating on both cells was good.

3.3. Effects of CSZP-coated Ti implant on osteogenesis differentiation of BMMSCs

In Fig. 3A, the mRNA expression of osteogenesis related factors in BMMSCs on CSZP coating, such as *ALP*, *COL1*, *OCN* and *RUNX2*, were all significantly higher than that on the Ti implants. Interestingly, mRNA expression of *ALP* from the CSZP coated-implants, an early stage osteogenesis marker, was 4-fold higher than that on Ti scaffolds. However, the mRNA expression of *OCN* on CSZP coating, a late stage osteogenesis marker, was 7-fold higher than that on Ti. Therefore, CSZP coating could induce osteogenesis of BMMSCs from the early stage and further promote the osteogenic process.

The result of protein expression of *ALP* and *OCN* by IF staining also supported the above idea. The expression of *ALP* in BMMSCs cultured for 7 days and that of *OCN* for 14 days on Ti and CSZP coating were



(caption on next page)

Fig. 6. Results of the in vivo bone-repairing model.

A. Sagittal, transverse, coronal, and 3D images of Micro-CT.

B. Quantitative analysis of Micro-CT data: BV/TV%, Tb.Th, and Tb.N respectively.

C. HE, Toluidine blue and Alizarin red-Calcein staining of hard tissue slides.

D. Summary of HE, Toluidine blue and Alizarin red-Calcein staining. (For interpretation of the references to colour in this figure legend, the reader is referred to the web version of this article.)

tested by IF staining. At day 7, BMMSCs exhibited a polygon-like shape and expressed ALP in the cytoplasm on Ti and CSZP coating preparations. On day 14, BMMSCs displayed an enlarged polygon-like shape, with increased cell numbers and OCN expression in the cytoplasm on Ti and CSZP coating. The expression of ALP and OCN in BMMSCs on CSZP coating were significantly higher than that on Ti at days 7 and 14, respectively.

3.4. Role of IL-4 on BMMSCs osteogenesis and macrophages polarization in CSZP-coated Ti implants

After BMMSCs and macrophages were co-cultured on Ti and CSZP coating for 4 days, osteogenesis of BMMSCs and polarization of macrophages were analyzed in the co-culture system (Fig. 4). The expression of osteogenesis-related factors on CSZP+IL-4 were significantly higher than those of Ti, CSZP coating and Ti + IL-4 (Fig. 4A). Compared with Ti, CSZP coating induced increased expression of *CCR7* which was a marker of M1 polarization (Fig. 4B). CSZP coating also induced increased expression of *IL-1 β* which was secreted by M1 macrophages. However, IL-4 switched the polarization from M1 to M2 and increased the expression of *BMP2* on Ti and CSZP coating. The expression of *iNOS* and *CD206* on Ti + IL-4 and CSZP+IL-4 analyzed by IF-staining also supported the above mechanism proposed above. To determine the ratio of M1/M2 cells, we used a High Content Screening System (Opera Phenix, PerkinElmer, USA) to calculate the number of cells expressing *iNOS* or *CD206* on each group. As shown in Fig. 4C, the number of *iNOS*-positive cells decreased from 2249 in the Ti group to 245 in the Ti + IL-4 group. Similarly, the number of *iNOS*-positive cells decreased from 3175 in the CSZP coating group to 991 in the CSZP+IL-4 group. Furthermore, the number of cells expressing the M2 phenotype marker *CD206* was higher in the Ti + IL-4 or CSZP+IL-4 treated group than in the Ti or CSZP coating group.

3.5. In vivo subcutaneous implant model

In Fig. 5, the expression of osteogenesis related factors and immunological factors on the tissue surrounding the Ti and CSZP implants were analyzed. Samples containing BMMSCs, which had been co-cultured previously for two days, were inserted into the subcutaneous layer of the rat's back. A treatment of 10 ng IL-4 was injected into tissue surrounding the Ti implant from day 3 to day 7 after implantation. The expression of *ALP*, *COL1*, *OCN* and *RUNX2* in the Ti + IL-4 and CSZP+IL-4 treated rats were higher than that from Ti and CSZP coating, as a result of the injection of IL-4 (10 ng) in the surrounding tissue for 5 days (Fig. 5A). In addition, the expression of osteogenic genes was higher on CSZP+IL-4 treated rats than in those receiving Ti + IL-4, which indicated better osteogenesis properties of the CSZP coating. IL-4 decreased the expression of *CCR7* and increased the expression of *CD206* on Ti and CSZP implants, which indicated that IL-4 could induce macrophages polarization from M1 to M2. In addition, we found that the expression of *IL-1 β* was decreased and the expression of *BMP2* was increased under the CSZP+IL-4 conditions. The IF staining on frozen tissue slices showed that IL-4 could reverse the increased in M1 cells and induced M2 polarization, which was similar to the above results. Under HE staining, the thickness of fibrous layer surrounding the Ti implant was analyzed. The results showed that the fibrous layer on the CSZP implant was thicker compared with that on the Ti implant, although IL-4 treatment decreased the thickness of the layer on the CSZP

implant, demonstrating that IL-4 was a critical factor in regulating the inflammatory response on CSZP coating.

3.6. In vivo femur defect repair model

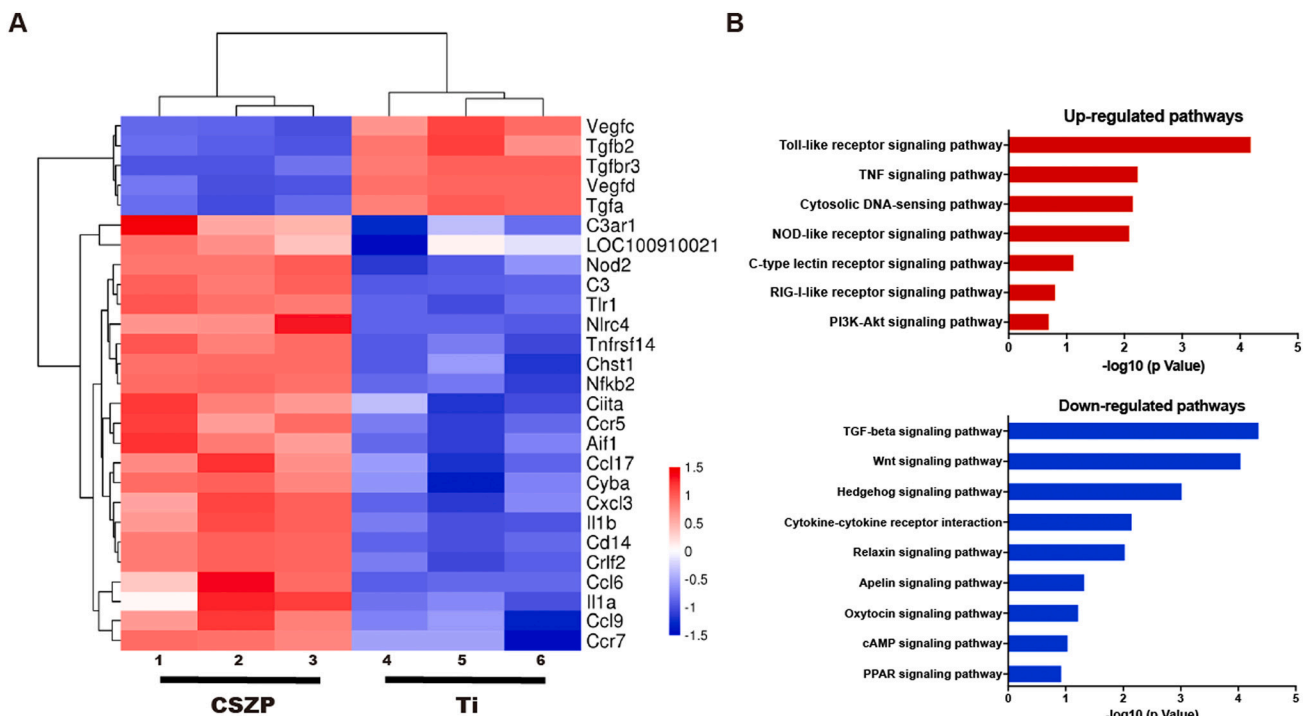
To assess the osseointegration effects of the Ti implant, these samples were implanted into femoral defects of rats for 6 weeks. IL-4 was injected into surrounding tissue of the implanted area from day 3 to day 7 after implantation in the Ti + IL-4 and CSZP+IL-4 groups.

Images revealing 2-D sagittal, transverse, and coronal views confirmed that bone formation through the delivery of IL-4 was significantly promoted in the CSZP+IL-4 and Ti + IL-4 groups (Fig. 6A). Quantitative statistical comparisons (Fig. 6B) demonstrated that the CSZP+IL-4 implant resulted in a significant increase in BV/TV (27.3% at 6 weeks). Moreover, CSZP+IL-4 implants caused the highest levels of Tb.N at 6 weeks (1.33 1/mm), and also increased Tb.Th at 6 weeks (0.23 mm). However, no significant differences were observed in BV/TV, Tb.Th, or Tb.N comparing the Ti and CSZP coating groups.

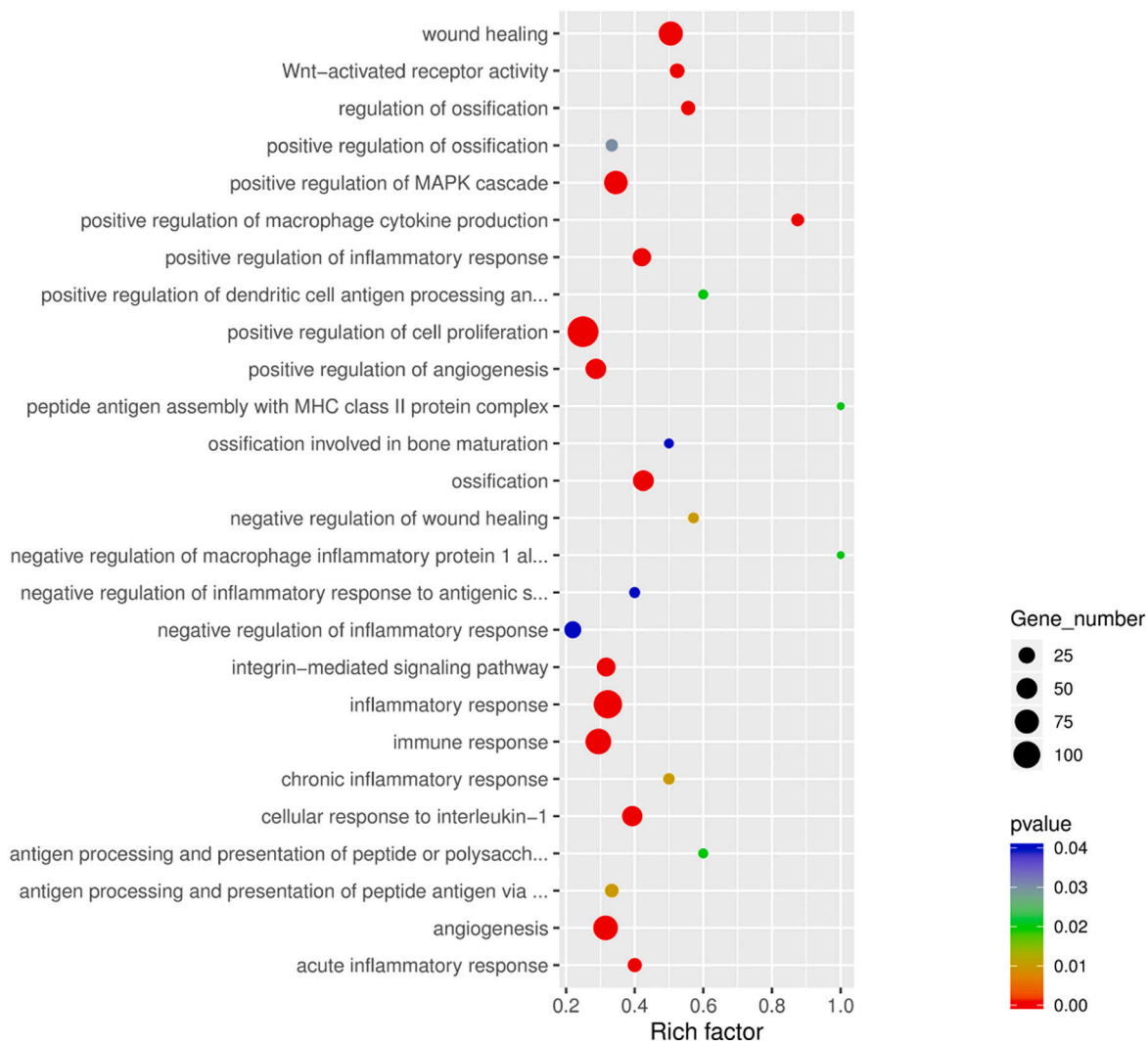
Quantitative analysis by micro-CT indicated the highest level of osteogenesis occurred in the CSZP+IL-4 group, followed by the Ti + IL-4 group (Fig. 6A and B), suggesting that CSZP+IL-4 had the strongest bone repair capability. Fig. 6C shows the bone adjacent to implants stained as pink (HE), blue (TB), red (Aliz.Red), and green (Calcein) areas, respectively. The results of HE and TB staining indicated that the bone mass surrounding the CSZP coating and Ti implants was limited, while the thickness of the fibrous layer had increased compared to tissue areas surrounding CSZP+IL-4 and Ti + IL-4 treated implants. The bone mass stained with HE or TB surrounding implants was quantified by the Positive area/Contact length ratio, which was higher in CSZP+IL-4 group than in the other groups (Fig. 6D). Calcein was labelled green on IF staining to indicate new bone formation from the week 2 week, and Aliz Red on IF staining (in red) revealed new bone formation after week 4. The expression of the 2-week label (green) was strongest in the CSZP+IL-4 treatment, followed by Ti + IL-4, Ti and CSZP-coated implants, respectively (Fig. 6D). However, the expression of 4-week label (red) was strongest in the CSZP+IL-4 implants, followed by CSZP, Ti + IL-4 and Ti implants (Fig. 6D). These results indicated that Ti was beneficial for bone formation at an early stage, while CSZP coating was beneficial for bone formation at the later stages, while CSZP+IL-4 improved bone formation continuously. The bone tissue tightly adhering to the surface of the CSZP+IL-4 implant, indicated the enhanced osseointegration surrounding the implants.

3.7. Gene expression of macrophages analyzed by microarray

Macrophages were seeded on Ti or CSZP coating for four days, followed by mRNA extraction for RNA sequencing. The expression of selected genes are illustrated by the heat map in Fig. 7A. Among the up-regulated genes were *CCR5* [21] and *CCR7* [22], both recognized as agonists of M1 polarization, and *IL-1 β* , which could be secreted following M1 polarization; expression of these genes were enhanced in the macrophages in the CSZP-coated scaffold condition compared with the bare Ti scaffold. The Toll-like receptor signaling pathway has been associated with facilitation of phagosome maturation and autophagy [23]. Toll-like and nod-like receptor signaling pathways have been reported to play an important role in M1 polarization for Ti-particle recognition [24]. C-type lectin and RIG-I-Like receptor signaling



C



(caption on next page)

Fig. 7. Gene expression analysis of macrophages cultured on scaffolds.

- A. Microarray heat map depicting the fold change in expression of selected genes.
 B. Representative top 7 upregulated and 9 downregulated pathways analyzed by KEGG pathway method.
 C. Statistics of GO Enrichment.

pathways have both been demonstrated to be pro-inflammation factors [25]. These inflammatory-related signaling pathways, toll-like, nod-like, C-type lectin and RIG-I-Like receptor signaling pathways, were all upregulated in CSZP macrophages (Fig. 7B). Conversely, down-regulated signaling pathways including TGF-beta [26], Wnt [27] and Hedgehog [28] have all been reported to promote M2 polarization. Fig. 7C shows the differential gene expression observed in macrophages co-cultured on CSZP coating and Ti and indicates the affected genes are involved in a variety of mechanisms that include osteogenesis, angiogenesis, and the immune response, and thus supports the importance of osteoimmunomodulation in this process.

4. Discussion

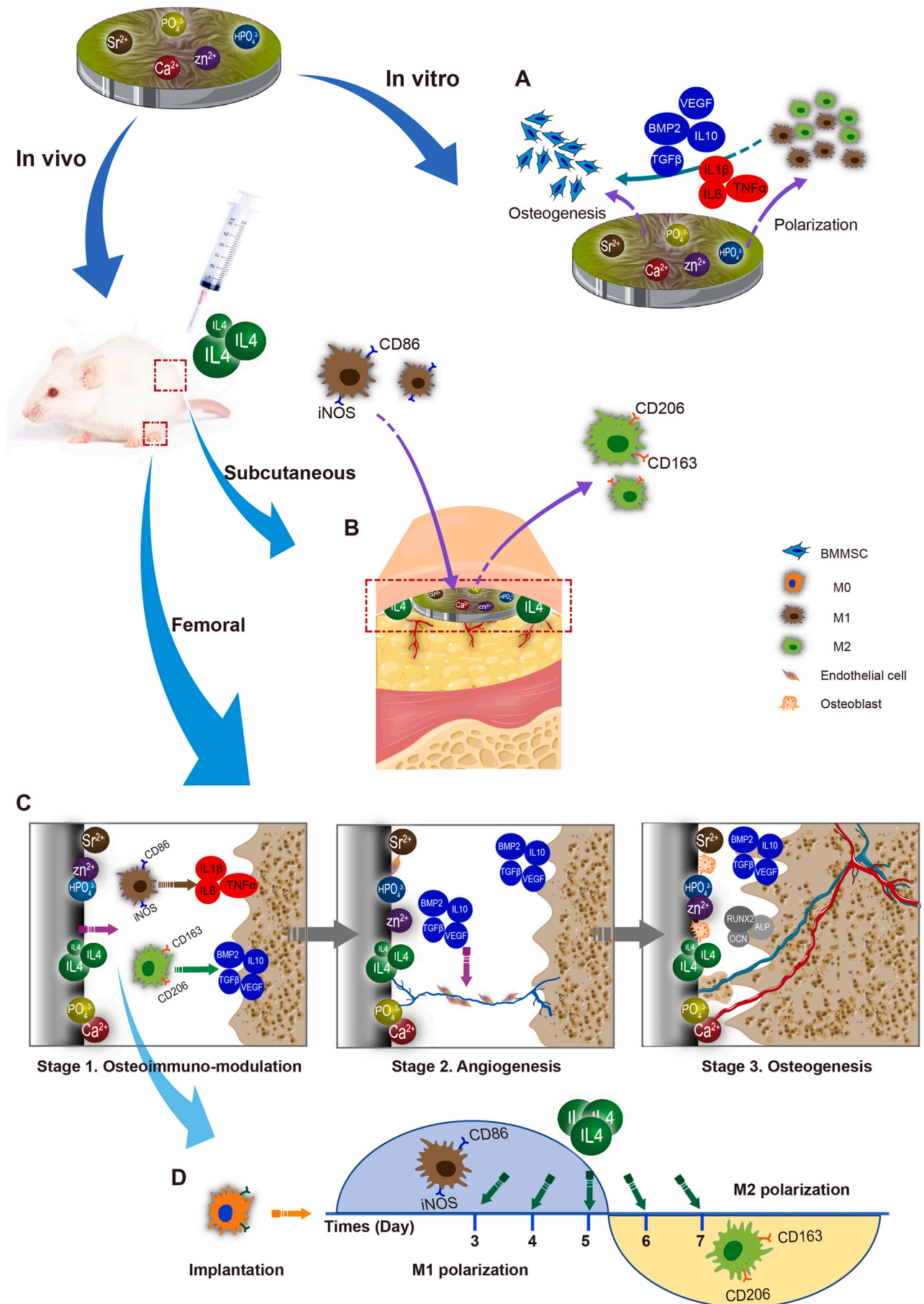
Surface modification is a reliable approach to obtain specific material properties and favorable outcomes for promoting osseointegration of Ti implants. Our team has successfully developed controllable preparations of phosphate coatings on the surface of Ti alloys with different micro-nano structures and elemental compositions in previous studies, which have demonstrated good biocompatibility and osteogenic properties *in vitro* [11,29,30]. However, the peripheral bone immune microenvironment interference with the surface properties of Ti implant is considered an important factor affecting implantation success rates. Due to their specific biological effects, metal ions phosphates have received widespread attention in the field of surface modification of metallic medical materials [10,31–33]. For example, Sr can improve early bone formation of the phosphate coating on the Ti implant surface, while its specific role and mechanism in osteoimmunomodulation requires further research. Therefore, the purpose of this study was to investigate the role of bioactive metal phosphate coatings of Ti implants in osteoimmunomodulation. Specifically, in this study, the effects of micro-nano structure and biological functional elements contained in the phosphate coating on the functional expression of BMMSCs and the polarization state expression of macrophage were studied.

PCC is the main method used for preparing phosphate coatings on Ti implant surfaces due to a series advantages, including high coating-substrate bonding strength, simple equipment and technology, satisfactory coating integrity, and the ability to achieve double accurate control of morphology and element composition [31]. In this study, we prepared the CSZP coating on Ti implants using the PCC method. The coating consists of micellar lamellar crystals, which form a specific micro-nano structure morphology. The main elements of the composition and corresponding atomic ratio is Sr:Ca:P = 2:1:3, in addition to a small amount of Zn. Meanwhile, each element is evenly distributed on the surface of the CSZP coating. The uniform distribution of the element composition ensures the uniformity of the distribution of phosphates in different phases on the surface of the CSZP coating, thereby ensuring the uniformity of the micro-nano structure morphology of the coating, so that cells attached to any position of the coating are consistently affected by the material. From a morphological perspective, the micro-nano structure of the CSZP coating and its crystal aggregation state induced better effects on osseointegration. Specifically, the CSZP coating was composed of a multi-layer stacking of lamellar crystals. The coating was uniform, complete and dense on the whole, while the lamellar crystals were three-dimensionally interlaced and with gaps between them observed on a microscopic level. Such crystal morphology and aggregation state endows the CSZP coating with loose and rough surface characteristics and good hydrophilicity. According to the test results, the roughness (Ra) value of CSZP coating was 20 times higher

than that of bare Ti, and the wettability significantly improved, while the water contact angle was only 1/2 of that of bare Ti. Therefore, this rough and hydrophilic micro-nano hierarchical structure is conducive to cell adhesion and provides more focus points for pseudopodia growth, especially allowing cellular filamentous pseudopodia to be embedded into the micro-nano space of lamellar crystals, allowing the formation of firm focal adhesion with the surface of the coating, to further promote cell adhesion and extension, and improve bone integration [29]. In terms of chemical composition, the CSZP coating contained functional metal elements Ca, Sr, Zn in a preparation that permitted their sustained and slow release. Studies have demonstrated that Ca, Sr and Zn ions and their phosphates have the effects of promoting bone formation and immune regulation. Calcium phosphate is the main inorganic component of bone tissue, and its various phase forms (including hydroxyapatite, β -tricalcium phosphate, brushite, etc.) all show excellent inherent biocompatibility and osseointegration properties [29,34–36]. Chen et al. [9] and Wang et al. [37] found that the strontium phosphate (including strontium apatite, strontium hydrogen phosphate) coatings on the surface of a magnesium (Mg) alloy can promote proliferation and differentiation of human mesenchymal stem cells and MC3T3E1 cells *in vitro*, as well as induce further bone formation *in vivo*. It has also been reported that the Sr-loaded phase-transited lysozyme (PTL) coating invokes greater osteogenesis ability by its effects on the immune environment due to the constant release of Sr ions directly at the implant-tissue interface [38]. Su et al. [39] discovered that the Zn ion that exist in the form of zinc phosphate, plays a key role in improving osseointegration and immune regulation. The immune microenvironment produced by the micro/nanostructured TiO₂/ZnO coating also showed better capacity to promote osteogenesis macroporous than the TiO₂ coating, which indicated that Zn ion plays an important role in osteoimmunomodulation [40]. Consequently, the CSZP coating used in this study has the potential to exhibit the desired osseointegration and osteoimmunomodulation ability due to the beneficial dual combination of its micro-nano structure and functional elements.

As expected, the *in vitro* cell adhesion fluorescence staining and SEM images indicated that macrophages and BMMSCs on the CSZP coating exhibited a wider range of spreading and adhesion, while no significant differences in cell proliferation or apoptosis were observed compared with bare Ti, which strongly indicated that the CSZP coating has good biocompatibility. In addition, this study also shows that the CSZP coating can induce osteogenic differentiation of BMMSCs, as representative osteogenic factors of BMMSCs deposited on the CSZP coating were significantly enhanced at both mRNA and protein levels. In light of the above evidence, three fundamental mechanisms may be involved: (i) the micro-nano surface morphology of CSZP can directly promote osteogenesis of BMMSCs [41]; (ii) Sr, Ca, and Zn elements exert a positive effect on proper cellular function and bone formation [42–44]; and (iii) the fate of cells is controlled by the hardness and geometry of their adhesive environment, possibly through forces localized at the adhesion sites [45]. More extended cell pseudopodia formed on CSZP coating than that on bare Ti may be responsible for the observed up-regulated expression of osteogenic factors.

The classic wound-healing process is a dynamic process consisting of hemostasis, inflammation, proliferation, and remodeling [46]. Hemostasis and the release of pro-inflammatory cytokines that attract immune cells can be marked as the initiation of the inflammatory phase. During the inflammatory phase, several pro-inflammatory cytokines (IL-6 and TNF- α) are secreted to recruit neutrophils and monocytes, which differentiate into macrophages [47]. These



(caption on next page)

Scheme 1. Flow diagram of the experimental procedure.

- A. In vitro BMMSCs and macrophages seeded on CSZP coated Ti implants exposed to IL-4 treatment.
- B. Schematic representation of M2 polarization processes in the subcutaneous implant model.
- C. Schematic representation of osteogenesis processes mediated by the surface physicochemical properties in vivo bone-repairing model.
- D. Schematic representation of macrophage polarization trend mediated by IL-4 delivery.

macrophages probably exhibit a pro-inflammatory M1 phenotype during this phase and phagocytose debris and dead neutrophils [48]. Further, M1 provide an ongoing source of inflammatory cytokines, such as IL-1 α , IL-1 β and IL-6, which are not only responsible for the control of macrophage recruitment and migration, but also are important for initiating the cascade of the inflammation response [22]. Compared with bare Ti, the CSZP coating induced an increased expression of *CCR7* and *IL-1 β* [49], indicating that the CSZP coating could induce M1 polarization and M1 recruitment during the inflammatory phase. The levels of inflammatory cytokines started to decline from the third day post-implantation [50]. From then on, M2 macrophages produce higher amounts of osteogenic, angiogenic, and anti-inflammatory cytokines (i.e., BMP2, BMP4, VEGF, TGF β , and IL-10) [51] to suppress inflammation, and contribute to bone regeneration [52,53]. The delivery of IL-4 was performed from the third day post-implantation as in previous studies [18], when M2 started to promote bone regeneration. The results of our work demonstrated that both CSZP + IL-4 and Ti + IL-4 exhibited the ability to promote M2 polarization and bone tissue regeneration.

During the process of bone regeneration, it is very important to create an environment which is conducive to the anti-inflammatory and osteogenesis of biomaterials via biomaterials modification [54–56]. Macrophages play a key role in all phases of wound healing and orchestrate the bone formation process. During the early phase, M1 exert pro-inflammatory functions. The results from our study showed that the surface morphology and the constituents of the CSZP coating could promote osteogenesis of BMMSCs and the secretion of IL-1 β , which is an important cytokine in macrophage recruitment, M1-phenotype differentiation, and phagocytosis of debris (Scheme 1A). During the later phase, M2 exert anti-inflammatory and regenerative functions such as BMP2 and IL-10 release, tissue repair, and regeneration (Scheme 1B and C). In the femoral defect model, IL-4 decreases inflammatory damage by inducing M2 polarization to create an osteogenic environment at stage 1. Then at stage 2, M2 secreted factors promote angiogenesis and provide basic support for osteogenesis. Finally, BMMSCs are differentiated to osteoblasts and the stable osseointegration of Ti implant is established at stage 3 (Scheme 1).

In this study, the CSZP coating recruited and induced M1 polarization. Adding IL-4 at an appropriate time (at day 3 post-implantation) induced M2 polarization and secretion of osteogenic cytokines (BMP2). The supplementary effect of both CSZP coating and IL-4 promoted bone repair and regeneration both in vitro and in vivo. With the delivery of IL-4, CSZP + IL-4 became an excellent osteoimmunomodulatory biomaterial both during the early and late phase of wound healing and tissue regeneration. Regarding the mechanism involved in IL-4-induced M2 polarization, it has been reported that JNK and its downstream effector c-Myc are involved in M2 polarization. Moreover, inhibition of JNK suppressed the M2 polarization, as well as a decreased level in c-Myc expression [57]. The mechanism of IL-4 in inducing M2 polarization may be an important issue that needs to be explored in the future.

CRedit authorship contribution statement

Da-Wang Zhao and Kang-Qing Zuo performed most of the experiments, prepared the figures, and wrote original manuscript. Kai Wang and Zhao-Yang Sun performed some of the experiments and data curation. Yu-Peng Lu provided advice and revised the manuscript for intellectual content. Lei Cheng, Gui-Yong Xiao, and Chao Liu performed project administration, experiments design, results interpretation, and

supervision. All authors approved the final version of the manuscript.

Declaration of competing interest

The authors declare that they have no known competing financial interests or personal relationships that could have appeared to influence the work reported in this paper.

Acknowledgement

Funding: This work was supported by Key R & D Projects of Shandong Province (Grant nos. 2019GSF108029), Dezhou Development and Reform Commission (Grant nos. 2019.124), Shandong Provincial Natural Science Foundation (Grant nos. ZR2017MEM014 and 2017G006010), Clinical Science and Technology Innovation Plan of Jinan (Grant nos. 201805052).

Data availability statement

All data generated or analyzed during this study are included in this article.

References

- [1] Q. Chen, G.A. Thouas, Metallic implant biomaterials, *Mater. Sci. Eng. R. Rep.* 87 (2015) 1–57.
- [2] M. Kaur, K. Singh, Review on titanium and titanium based alloys as biomaterials for orthopaedic applications, *Mater. Sci. Eng. C Mater. Biol. Appl.* 102 (2019) 844–862.
- [3] C. Hu, D. Ashok, D.R. Nisbet, V. Gautam, Bioinspired surface modification of orthopedic implants for bone tissue engineering, *Biomaterials* 219 (2019) 119366.
- [4] W. Liu, S. Liu, L. Wang, Surface modification of biomedical titanium alloy: micro-morphology, microstructure evolution and biomedical applications, *Coatings* 9 (4) (2019) 249.
- [5] E.J. Tobin, Recent coating developments for combination devices in orthopedic and dental applications: a literature review, *Adv. Drug Deliv. Rev.* 112 (2017) 88–100.
- [6] S. Spriano, S. Yamaguchi, F. Baimo, S. Ferraris, A critical review of multifunctional titanium surfaces: new frontiers for improving osseointegration and host response, avoiding bacteria contamination, *Acta Biomater.* 79 (2018) 1–22.
- [7] B.N. Brown, B.D. Ratner, S.B. Goodman, S. Amar, S.F.J.B. Badylak, Macrophage Polarization: An Opportunity for Improved Outcomes in Biomaterials and Regenerative Medicine, 33(15) (2012), pp. 3792–3802.
- [8] J.R. Alhamdi, T. Peng, I.M. Alnaggar, K.L. Hawley, K.L. Spiller, L.T.J.B. Kuhn, Controlled M1-to-M2 Transition of Aged Macrophages by Calcium Phosphate Coatings, 196 (2019), pp. 90–99.
- [9] X.B. Chen, D.R. Nisbet, R.W. Li, P.N. Smith, T.B. Abbott, M.A. Easton, D.H. Zhang, N. Birbilis, Controlling initial biodegradation of magnesium by a biocompatible strontium phosphate conversion coating, *Acta Biomater.* 10 (3) (2014) 1463–1474.
- [10] Y. Su, K. Wang, J. Gao, Y. Yang, Y.-X. Qin, Y. Zheng, D. Zhu, Enhanced cytocompatibility and antibacterial property of zinc phosphate coating on biodegradable zinc materials, *Acta Biomater.* 98 (2019) 174–185.
- [11] B. Liu, X.-m. Shi, G.-y. Xiao, Y.-p. Lu, In-situ preparation of scholizite conversion coatings on titanium and Ti-6Al-4V for biomedical applications, *Colloids Surf. B: Biointerfaces* 153 (2017) 291–299.
- [12] X.-c. Zhao, G.-y. Xiao, X. Zhang, H.-y. Wang, Y.-p. Lu, Ultrasonic induced rapid formation and crystal refinement of chemical converted hopeite coating on titanium, *J. Phys. Chem. C* 118 (4) (2014) 1910–1918.
- [13] T. Mokabber, H.T. Cao, N. Norouzi, P. Van Rijn, Y.T. Pei, Interfaces, antimicrobial electrodeposited silver-containing calcium phosphate coatings, 12(5) (2020), pp. 5531–5541.
- [14] J.Y. Reginster, M.L. Brandi, J. Cannata-Andia, C. Cooper, B. Cortet, J.M. Feron, H. Genant, S. Palacios, J.D. Ringe, R. Rizzoli, The position of strontium ranelate in today's management of osteoporosis, *Osteoporos. Int.* 26 (6) (2015) 1667–1671.
- [15] S. Hojyo, T. Fukada, Roles of zinc signaling in the immune system, *J Immunol Res* 2016 (2016) 6762343.
- [16] R. Marsell, T.A. Einhorn, The biology of fracture healing, *Injury* 42 (6) (2011) 551–555.
- [17] S. Franz, S. Rammelt, D. Scharnweber, J.C. Simon, Immune responses to implants - a review of the implications for the design of immunomodulatory biomaterials, *Biomaterials* 32 (28) (2011) 6692–6709.
- [18] Z.W. Zheng, Y.H. Chen, D.Y. Wu, J.B. Wang, M.M. Lv, X.S. Wang, J. Sun,

- Z.Y. Zhang, Development of an accurate and proactive immunomodulatory strategy to improve bone substitute material-mediated osteogenesis and angiogenesis, *Theranostics* 8 (19) (2018) 5482–5500.
- [19] B. Liu, G.-y. Xiao, C.-c. Jiang, Y.-z. Zheng, L.-l. Wang, Y.-p. Lu, Formation initiation and structural changes of phosphate conversion coating on titanium induced by galvanic coupling and Fe²⁺ ions, *RSC Adv.* 6 (79) (2016) 75365–75375.
- [20] F.A. Jacobs, M. van de Vyver, W.F. Ferris, Isolation and characterization of different mesenchymal stem cell populations from rat femur, *Methods Mol. Biol.* 1916 (2019) 133–147.
- [21] J.H. Huh, H.M. Kim, E.S. Lee, M.H. Kwon, B.R. Lee, H.J. Ko, C.H. Chung, Dual CCR2/5 antagonist attenuates obesity-induced insulin resistance by regulating macrophage recruitment and M1/M2 status, *Obesity (Silver Spring)* 26 (2) (2018) 378–386.
- [22] A. Shapouri-Moghaddam, S. Mohammadian, H. Vazini, M. Taghadosi, S.A. Esmaeili, F. Mardani, B. Seifi, A. Mohammadi, J.T. Afshari, A. Sahebkar, Macrophage plasticity, polarization, and function in health and disease, *J. Cell. Physiol.* 233 (9) (2018) 6425–6440.
- [23] M.A. Sanjuan, C.P. Dillon, S.W. Tait, S. Moshiah, F. Dorsey, S. Connell, M. Komatsu, K. Tanaka, J.L. Cleveland, S. Withoff, D.R. Green, Toll-like receptor signalling in macrophages links the autophagy pathway to phagocytosis, *Nature* 450 (7173) (2007) 1253–1257.
- [24] J. Pajarinen, V.P. Kouri, E. Jamsen, T.F. Li, J. Mandelin, Y.T. Kontinen, The response of macrophages to titanium particles is determined by macrophage polarization, *Acta Biomater.* 9 (11) (2013) 9229–9240.
- [25] X. Zhao, H. Chu, B.H. Wong, M.C. Chiu, D. Wang, C. Li, X. Liu, D. Yang, V.K. Poon, J. Cai, J.F. Chan, K.K. To, J. Zhou, K.Y. Yuen, Activation of C-type Lectin receptor and (RIG)-I-like receptors contributes to proinflammatory response in Middle East respiratory syndrome coronavirus-infected macrophages, *J. Infect. Dis.* 221 (4) (2020) 647–659.
- [26] L. Zhu, X. Fu, X. Chen, X. Han, P. Dong, M2 macrophages induce EMT through the TGF-beta/Smad2 signaling pathway, *Cell Biol. Int.* 41 (9) (2017) 960–968.
- [27] H. Sha, D. Zhang, Y. Zhang, Y. Wen, Y. Wang, ATF3 promotes migration and M1/M2 polarization of macrophages by activating tenascinC via Wnt/betacatenin pathway, *Mol. Med. Rep.* 16 (3) (2017) 3641–3647.
- [28] A.J. Petty, A. Li, X. Wang, R. Dai, B. Heyman, D. Hsu, X. Huang, Y. Yang, Hedgehog signaling promotes tumor-associated macrophage polarization to suppress intratumoral CD8+ T cell recruitment, *J. Clin. Invest.* 129 (12) (2019) 5151–5162.
- [29] B. Liu, Y.-y. Guo, G.-y. Xiao, Y.-p. Lu, Preparation of micro/nano-fibrous brushite coating on titanium via chemical conversion for biomedical applications, *Appl. Surf. Sci.* 399 (2017) 367–374.
- [30] B. Liu, G.-y. Xiao, C.-z. Chen, Y.-p. Lu, X.-w. Geng, Hopeite and scholite coatings formation on titanium via wet-chemical conversion with controlled temperature, *Surf. Coat. Technol.* 384 (2020) 125330.
- [31] B. Liu, X. Zhang, G.-y. Xiao, Y.-p. Lu, Phosphate chemical conversion coatings on metallic substrates for biomedical application: a review, *Mater. Sci. Eng. C* 47 (2015) 97–104.
- [32] H. Shi, T. Wu, J. Zhang, X. Ye, S. Zeng, X. Liu, T. Yu, J. Ye, C. Zhou, Biocompatible beta-SrHPO₄ clusters with dandelion-like structure as an alternative drug carrier, *Mater. Sci. Eng. C Mater. Biol. Appl.* 81 (2017) 8–12.
- [33] P.-P. Zhao, H.-R. Hu, J.-Y. Liu, Q.-F. Ke, X.-Y. Peng, H. Ding, Y.-P. Guo, Gadolinium phosphate/chitosan scaffolds promote new bone regeneration via Smad/Runx2 pathway, *Chem. Eng. J.* 359 (2019) 1120–1129.
- [34] Y. Su, I. Cockerill, Y. Zheng, L. Tang, Y.X. Qin, D. Zhu, Biofunctionalization of metallic implants by calcium phosphate coatings, *Bioact. Mater.* 4 (2019) 196–206.
- [35] M. Gallo, B.L.G. Santoni, T. Douillard, F. Zhang, L. Gremillard, S. Dolder, W. Hofstetter, S. Meille, M. Bohner, J. Chevalier, S. Tadier, Effect of grain orientation and magnesium doping on beta-tricalcium phosphate resorption behavior, *Acta Biomater.* 89 (2019) 391–402.
- [36] C. Zhao, X. Wang, L. Gao, L. Jing, Q. Zhou, J. Chang, The role of the micro-pattern and nano-topography of hydroxyapatite bioceramics on stimulating osteogenic differentiation of mesenchymal stem cells, *Acta Biomater.* 73 (2018) 509–521.
- [37] Z. Wang, X. Wang, Y. Tian, J. Pei, J. Zhang, C. Jiang, J. Huang, Z. Pang, Y. Cao, X. Wang, S. An, X. Wang, H. Huang, G. Yuan, Z. Yan, Degradation and osteogenic induction of a SrHPO₄-coated Mg–Nd–Zn–Zr alloy intramedullary nail in a rat femoral shaft fracture model, *Biomaterials* 247 (2020).
- [38] X. Lu, W. Zhang, Z. Liu, S. Ma, Y. Sun, X. Wu, X. Zhang, P. Gao, Application of a strontium-loaded, phase-transited lysozyme coating to a titanium surface to enhance osteogenesis and osteoimmunomodulation, *Med. Sci. Monit.* 25 (2019) 2658–2671.
- [39] Y. Su, H. Yang, J. Gao, Y.X. Qin, Y. Zheng, D. Zhu, Interfacial zinc phosphate is the key to controlling biocompatibility of metallic zinc implants, *Adv. Sci.* 1900112 (2019).
- [40] R. Zhang, X. Liu, Z. Xiong, Q. Huang, X. Yang, H. Yan, J. Ma, Q. Feng, Z. Shen, The immunomodulatory effects of Zn-incorporated micro/nanostructured coating in inducing osteogenesis, *Artif. Cells Nanomed. Biotechnol.* 46 (sup1) (2018) 1123–1130.
- [41] W. Zhang, G. Wang, Y. Liu, X. Zhao, D. Zou, C. Zhu, Y. Jin, Q. Huang, J. Sun, X. Liu, X. Jiang, H. Zreiqat, The synergistic effect of hierarchical micro/nano-topography and bioactive ions for enhanced osseointegration, *Biomaterials* 34 (13) (2013) 3184–3195.
- [42] L. Mao, L. Xia, J. Chang, J. Liu, L. Jiang, C. Wu, B. Fang, The synergistic effects of Sr and Si bioactive ions on osteogenesis, osteoclastogenesis and angiogenesis for osteoporotic bone regeneration, *Acta Biomater.* 61 (2017) 217–232.
- [43] C.B. Danoux, D.C. Bassett, Z. Othman, A.I. Rodrigues, R.L. Reis, J.E. Barralet, C.A. van Blitterswijk, P. Habibovic, Elucidating the individual effects of calcium and phosphate ions on hMSCs by using composite materials, *Acta Biomater.* 17 (2015) 1–15.
- [44] S. An, Q. Gong, Y. Huang, Promotive effect of zinc ions on the vitality, migration, and osteogenic differentiation of human dental pulp cells, *Biol. Trace Elem. Res.* 175 (1) (2017) 112–121.
- [45] M. Macis, F. Lugli, F. Zerbetto, Modeling living cells response to surface tension and chemical patterns, *ACS Appl. Mater. Interfaces* 9 (23) (2017) 19552–19561.
- [46] B. Mahdavian Delavary, W.M. van der Veer, M. van Egmond, F.B. Niessen, R.H. Beelen, Macrophages in skin injury and repair, *Immunobiology* 216 (7) (2011) 753–762.
- [47] G.J. Kotwal, S. Chien, Macrophage differentiation in normal and accelerated wound healing, *Results Probl. Cell Differ.* 62 (2017) 353–364.
- [48] Z. Julier, A.J. Park, P.S. Briquez, M.M. Martino, Promoting tissue regeneration by modulating the immune system, *Acta Biomater.* 53 (2017) 13–28.
- [49] M. Jaguin, N. Houlbert, O. Fardel, V. Lecreur, Polarization profiles of human M-CSF-generated macrophages and comparison of M1-markers in classically activated macrophages from GM-CSF and M-CSF origin, *Cell. Immunol.* 281 (1) (2013) 51–61.
- [50] R.A. Bank, J. Zandstra, H. Room, A.H. Petersen, S.M. van Putten, Biomaterial encapsulation is enhanced in the early stages of the foreign body reaction during conditional macrophage depletion in transgenic macrophage Fas-induced apoptosis mice, *Tissue Eng. Part A* 23 (19–20) (2017) 1078–1087.
- [51] F. Loi, L.A. Cordova, J. Pajarinen, T.H. Lin, Z. Yao, S.B. Goodman, Inflammation, fracture and bone repair, *Bone* 86 (2016) 119–130.
- [52] Z.T. Chen, T. Klein, R.Z. Murray, R. Crawford, J. Chang, C.T. Wu, Y. Xiao, Osteoimmunomodulation for the development of advanced bone biomaterials, *Mater. Today* 19 (6) (2016) 304–321.
- [53] D. Hachim, S.T. LoPresti, C.C. Yates, B.N. Brown, Shifts in macrophage phenotype at the biomaterial interface via IL-4 eluting coatings are associated with improved implant integration, *Biomaterials* 112 (2017) 95–107.
- [54] X. Li, M.L. Qi, X.L. Sun, M.D. Weir, F.R. Tay, T.W. Oates, B. Dong, Y.M. Zhou, L. Wang, H.H.K. Xu, Surface treatments on titanium implants via nanostructured ceria for antibacterial and anti-inflammatory capabilities, *Acta Biomater.* 94 (2019) 627–643.
- [55] T. Liu, Z. Zeng, Y. Liu, J. Wang, M.F. Maitz, Y. Wang, S.H. Liu, J.Y. Chen, N. Huang, Surface modification with dopamine and heparin/poly-L-lysine nanoparticles provides a favorable release behavior for the healing of vascular stent lesions, *ACS Appl. Mater. Interfaces* 6 (11) (2014) 8729–8743.
- [56] H.F. Qi, Q. Chen, H.L. Ren, X.L. Wu, X.H. Liu, T.L. Lu, Electrophoretic deposition of dexamethasone-loaded gelatin nanospheres/chitosan coating and its dual function in anti-inflammation and osteogenesis, *Colloid Surf. B* 169 (2018) 249–256.
- [57] J. Hao, Y. Hu, Y. Li, Q. Zhou, X. Lv, Involvement of JNK signaling in IL4-induced M2 macrophage polarization, *Exp. Cell Res.* 357 (2) (2017) 155–162.